Eigenfunctions in one-dimensional disordered systems. II. Results and discussion*

C. Papatriantafillou and E. N. Economou
Department of Physics, University of Virginia, Charlottesville, Virginia 22901
(Received 31 July 1975)

A formalism previously developed within the framework of Anderson's model for disordered lattices produces convenient expressions for transport-related averages of the type $\langle G^* G \rangle_{av}$ (G is the Green's function of the system). Those expressions involve a probability distribution function that satisfies an integral equation. The probability distribution function is obtained by solving numerically the integral equation for systems with "rectangular distribution" type of randomness, and is subsequently used to calculate the corresponding transport-related quantities. The results, which provide detailed information about the eigenfunctions at different energies and degrees of randomness, are analyzed and discussed.

I. INTRODUCTION

In a previous paper,[1] hereafter referred to as I, we developed and presented a formalism suitable for the study of transport-related problems in one-dimensional (1-D) disordered systems. Such a study is important both from a theoretical point of view and in view of the existence and ongoing experimental and theoretical study of a whole class of metallo-organic materials exhibiting quasi-one-dimensional behavior and, in some cases, peculiar transport and magnetic properties.[2-4] The difficulty of the problem is considerable, and little has been done for its study from first principles.[5,6] The formalism developed in I makes possible for the first time the numerical calculation of quantities of the type $\langle GG^* \rangle_{av}$, where G is the Green's function of the system and $\langle\ \rangle_{av}$ denotes average over all configurations. A wealth of information, relating to localization of the eigenstates and transport properties of the system, is directly obtainable from such quantities.

The formalism presented in I expresses those $\langle GG^* \rangle_{av}$ quantities in terms of the joint probability distribution of the real and imaginary part of the Green's function. The said probability distribution is obtained as solution of an integral equation. The integral equation is also derived in I and the form of the solution is studied analytically, and explained qualitatively in terms of the mathematical properties of the Green's functions and their probability distributions. Finally, in Sec. III of I a number of quantities of physical interest are introduced and defined. Those quantities relate to the localized character of the eigenstates of the system, have mostly the form of "characteristic" or "localization" lengths, and are directly related to the $\langle GG^* \rangle_{av}$ quantities. The knowledge of the localization lengths, apart from revealing the form of the eigenstates of the system, is also essential to most phenomenological studies of the transport properties of the system. For example, in the phonon-assisted hopping conduction[7] theory the overlap between localized eigenstates is required. Then that overlap is expressed through a characteristic length which is assumed to be the same as the length R_d that characterizes the rate of decay of the eigenstates at infinity. In fact, the length R_d exclusively determines the overlap when the two eigenstates are so far apart that only their extreme tails overlap, i.e., when their eigenenergies differ infinitesimally. However, when considering transitions between states with finite eigenenergy difference, the eigenstates may be much closer and their overlap should be determined by a length characterizing the extent of their appreciable part and not of their tails. This length may be in some cases widely different than R_d. Our results indeed suggest such wide differences, mainly in the cases of weakly disordered systems.

In the present paper we use the formalism developed in I to calculate numerically the transport-related quantities introduced in Sec. III of I and briefly discussed above. Consequently, in Sec. II we present the basic formulas required for our calculations, conveniently transformed to facilitate numerical solutions. In Sec. III we study the case of a system with a rectangular distribution, or Anderson, type of disorder; in Sec. III A we obtain the corresponding joint probability distribution function by solving numerically for different energies and degrees of disorder the integral equation it obeys. Then in Sec. III B we use the obtained numerical solutions to calculate the $\langle GG^* \rangle_{av}$ quantities at the corresponding energies and degrees of disorder. Finally, we use the calculated values of the $\langle GG^* \rangle_{av}$ quantities to calculate, in Sec. IV A, the different localization lengths that characterize the form of the eigenstates in a disordered system and to study, in Sec. IV B, the diffusibility of a particle placed initially on a lattice site of the disordered system. Our results are discussed and physically interpreted.

II. BASIC FORMULAS

We consider a 1-D Anderson model described by a Hamiltonian of the form

$$\langle l|H|m\rangle = \epsilon_l \delta_{lm} + V(\delta_{m,l+1} + \delta_{m,l-1}) , \tag{2.1}$$

where $|l\rangle$ is an atomiclike orbital centered around the lattice point l ($l = 0, \pm 1, \pm 2, \ldots$), ϵ_l are independent random variables having a common probability distribution $P_0(\epsilon_l)$, and V is a positive constant. The Green's function $G_{00}(z) = \langle 0|(z-H)^{-1}|0\rangle$ can be written

$$G_{00}(z) = [z - \epsilon_0 - \Delta_0(z)]^{-1} , \tag{2.2}$$

which relation defines the so-called self-energy $\Delta_0(z)$ at site 0. Then $\Delta_0(z)$ is in turn expressed through the quantities $\tau_0^+(E)$, $\theta_0^+(E)$, $\tau_0^-(E)$, and $\theta_0^-(E)$, in the form

$$\Delta_0(E+is) \to \tau_0^+(E) + \tau_0^-(E) - is[\theta_0^+(E) + \theta_0^-(E)] , \tag{2.3}$$

as $s \to 0$. The quantities τ and θ are defined and the above-outlined formalism is rigorously presented in Sec. IV of I where the formalism proceeds to the derivation of two integral equations. The first is obeyed by the probability distribution[8,9] $f(\tau)$ of the random variables $\tau^+(E)$ or $\tau^-(E)$, and the second is obeyed by the joint probability distribution $P(\tau, \theta)$ of the pairs $(\tau^+(E), \theta^+(E))$ or $(\tau^-(E), \theta^-(E))$ [see Sec. IV of I, relations 4.15 and 4.17 there].

Explicit expressions for the quantities $\langle GG^* \rangle_{\rm av}$ can be obtained involving the joint probability distribution P. Therefore it is necessary to solve the integral equation and obtain P. An analytic solution of the integral equation seems unfeasible. Consequently, and in view of the importance of its solution, a numerical-solution approach was taken; for that purpose the integral equation was properly transformed, by a change of variables, to facilitate the numerical procedure. The transformation $\tau = A + B\tan\phi$ (A and B appropriate constants) has been successfully used[9] to obtain numerically the probability $f(\tau)$ mentioned above. The same transformation is made here for τ, while for θ different transformations have been tried; finally the transformation $\theta = (\tan\omega)^2$ was chosen. Therefore by transforming $(\tau, \theta) \to (\phi, \omega)$,

$$\tau(\phi) = A + B\tan\phi , \qquad \theta(\omega) = (\tan\omega)^2 , \qquad \phi(\tau) = \arctan[(\tau - A)B^{-1}] , \tag{2.4}$$

the integral equation for $f(\tau)$ is transformed to

$$f(\phi) = B[\cos(\phi)\tau(\phi)]^{-2} \int_{-\pi/2}^{\pi/2} P_0(E - x - \tau^{-1}(\phi)) f(x)\, dx , \tag{2.5}$$

with the normalization condition

$$\int_{-\pi/2}^{\pi/2} f(\phi)\, d\phi = 1 , \tag{2.6}$$

where from now on we set $V = 1$ in order to simplify the forms, since V only defines the energy scale. The integral equation for $P(\tau, \theta)$ is also transformed to

$$P(\phi, \omega) = B[\cos(\phi)\cos(\omega)\tau(\phi)]^{-2} \{\theta(\omega) \times [-1 + \theta(\omega)\tau^{-2}(\phi)]\}^{-1/2} \times \int_{D^-}^{D^+} P_0(E - \tau(x) - \tau^{-1}(\phi)) \times P(x, \arctan\{[-1 + \theta(\omega)\tau^{-2}(\phi)]^{1/2}\})\, dx , \tag{2.7a}$$

where

$$D^{\pm} = \phi\{\pm[-1 + \theta(\omega)\tau^{-2}(\phi)]^{1/2}\} , \tag{2.7b}$$

with the normalization condition

$$\int_0^{\pi/2} P(\phi, \omega)\, d\omega = f(\phi) . \tag{2.8}$$

As mentioned before, the probability distributions $f(\phi)$ and $P(\phi, \omega)$ can be used to calculate a number of ensemble averages of quantities of interest. For example, $f(\phi)$ has been used[9] to calculate, among other things, the average density of states per site $\rho(E)$ of the system. Likewise, $P(\phi, \omega)$ can be used to calculate quantities of the type $\langle GG^* \rangle_{\rm av}$ and more specifically

$$\langle \zeta_{0l}(E) \rangle_{\rm av} = \left\langle \lim_{s\to 0} (s/\pi) G_{0l}(E+is) G_{l0}(E-is) \right\rangle_{\rm av} . \tag{2.9}$$

Such quantities can be calculated from $P(\phi, \omega)$ in a fashion described in Sec. V of I [see relations (5.5) and (5.12)–(5.14) there]. Of course those relations also have to be properly transformed to facilitate the numerical procedure, and we have

$$\langle \zeta_{00}(E) \rangle_{\rm av} = \int_{-\pi/2}^{\pi/2} d\phi^+ d\phi^- \int_0^{\pi/2} d\omega^+ d\omega^- \times P_0(E - \tau(\phi^+) - \tau(\phi^-)) P(\phi^+, \omega^+) P(\phi^-, \omega^-) \times [1 + \theta(\omega^+) + \theta(\omega^-)]^{-1} . \tag{2.10}$$

Also, the successive ζ_{0l} can be obtained from successive $Z_l(\phi, \omega)$, obtained by the following algorithm for $l = 1, 2, \ldots$:

$$Z_0(\phi, \omega) = \int_0^{\pi/2} P(\phi, y)[1 + \theta(\omega) + \theta(y)]^{-1}\, dy , \tag{2.11}$$

$$Z_1(\phi, \omega) = B[\cos(\phi)\tau(\phi)]^{-2} \int_{-\pi/2}^{\pi/2} P_0(E - \tau(x) - \tau^{-1}(\phi)) \times Z_0(x, \omega)\, dx , \tag{2.12}$$

$$Z_l(\phi, \omega) = B[\cos(\phi)\tau(\phi)]^{-2} \int_{-\pi/2}^{\pi/2} P_0(E - \tau(x) - \tau^{-1}(\phi)) Z_{l-1}(x, \arctan(\{\tau^{-2}(x) \times [1 + \theta(\omega)]\}^{1/2}))\, dx , \quad l > 1 . \tag{2.13}$$

Then ζ_{0l} is expressed through Z_l ($l = 1, 2, \ldots$) as

$$\langle \zeta_{0l}(E)\rangle = B^{-1}\int_{-\pi/2}^{\pi/2} d\phi \int_0^{\pi/2} d\omega \cos^2\left[\phi\left(\frac{1}{\tau(\phi)}\right)\right] \times P(\phi,\omega) Z_l\{\phi[1/\tau(\phi)],\omega\}, \quad l=1,2,\ldots. \tag{2.14}$$

In Sec. III we present the results obtained in the case of a random system with a rectangular probability distribution $P_0(\epsilon)$.

III. THE RECTANGULAR DISTRIBUTION CASE

A. Numerical solution of the integral equation

As discussed in Sec. II the type of disorder of the system is introduced in the Anderson model through the probability distribution of the set ϵ_i, the diagonal Hamiltonian elements [see relation (2.1)]. Throughout the present work we have assumed the ϵ_i to be independent random variables having a common probability distribution $P_0(\epsilon_i)$; therefore P_0 completely determines the type and degree of disorder of the random system. We present here the results obtained in the case of a rectangular distribution P_0 defined as

$$P_0(\epsilon_i) = 1/2\alpha \quad \text{for } |\epsilon_i| \le \alpha, \qquad P_0(\epsilon_i) = 0 \quad \text{otherwise}, \tag{3.1}$$

where α is a positive parameter solely defining P_0. Then, in the limit $\alpha \to 0$, $P_0(\epsilon_i) \to \delta(\epsilon_i)$ and we obtain the periodic system, while in the limit $\alpha \to \infty$ the system is so strongly disordered that its eigenstates become the atomiclike orbitals $|i\rangle$ centered around the lattice points i. Of course the $\alpha \to \infty$ case is trivially understood; the limit $\alpha \to 0$ is the extensively studied periodic case (although it is very interesting to study the way this periodic limit is achieved as $\alpha \to 0$). Therefore the interesting range of values for α is where the width of the distribution P_0 (being 2α) becomes comparable to the bandwidth of the periodic system (being 4, since we have assumed here $V=1$). Calculations[9] indicate that there is a gradual change of character in the system, from strongly localized to quasiperiodic, around the value $\alpha = 1$.

In Sec. IV of I the behavior of the joint probability distribution $P(\tau,\theta)$ was examined by studying the properties of the integral equation that P satisfies. It is shown there that $P(\tau,\theta)$ is nonzero inside the parabola $\theta = \tau^2$. For a terminated distribution $P_0(\epsilon)$, the nonzero values of $P(\tau,\theta)$ are restricted further and lie essentially between two parabolas $\theta = k_{\min}\tau^2$ and $\theta = k_{\max}\tau^2$ (where the constants k obey $k_{\max} > k_{\min} > 1$) for $|\tau| \gg 0$, while for $\tau \simeq 0$ the solution is nonzero for $\theta \gg 0$ and inside a finite portion of the positive θ axis. In Sec. IV of I it is also shown that $P(\tau,\theta) \propto \tau^{-4}$ as τ and θ go to infinity along lines $\theta = k\tau^2$. The above-described behavior of $P(\tau,\theta)$ is easily translated into a corresponding behavior for $P(\phi,\omega)$ introduced in Sec. II, by observing the transformations (2.4) and the correspondence

$$P(\phi,\omega) \leftrightarrow P(\tau,\theta)\frac{d\tau}{d\phi}\frac{d\theta}{d\omega}. \tag{3.2}$$

The parabolas $\theta = k\tau^2$ are also transformed into lines

$$\omega = \arctan(|A + B\tan\phi\,|\,k^{1/2}) \tag{3.3}$$

in the (ϕ,ω) plane.

With all the above in mind we proceeded to solve numerically the integral equation (2.7) for $P(\phi,\omega)$. For that purpose, the (ϕ,ω) plane $(-\frac{1}{2}\pi < \phi < \frac{1}{2}\pi$, $0 < \omega < \frac{1}{2}\pi)$ was subdivided into (typically) 100 subdivisions along each axis and $P(\phi,\omega)$ became a 100×100 matrix. Then the kernel of the integral equation was properly transformed into a discrete one, following the method used in Ref. 9, and a numerical solution of $P(\phi,\omega)$ was obtained by a converging iteration scheme,

$$P_{n+1} = K_0 P_n, \quad P_{n+1} - P_n \to 0, \quad \text{as } n \to \infty, \tag{3.4}$$

in a way essentially the same as that of Ref. 9. Our numerical accuracy was estimated to be around 10%.

The numerical solution requires the *a priori* knowledge of the behavior of $P(\phi,\omega)$ as $\omega \to \frac{1}{2}\pi$ (ω beyond the last subdivision) for a constant ϕ [the equivalent in $P(\tau,\theta)$ of $\theta \to \infty$ and constant τ]. This behavior is qualitatively known from the extensive analytic study of the solution $P(\tau,\theta)$ in I; moreover, this qualitative knowledge suffices because the solution proves insensitive to the exact form of the assumed behavior at $\omega \to \frac{1}{2}\pi$. This behavior actually influences only the negligibly small numerical values of $P(\phi,\omega)$ at a small percentage of points of the $P(\phi,\omega)$ matrix, around $\phi = 0$, $\omega = \frac{1}{2}\pi$ (this is a region where the solution should be essentially zero, as already pointed out).

The basic properties of the obtained solution are shown in Fig. 1. The shaded area indicates the appreciable values of $P(\phi,\omega)$. The obtained values of $P(\phi,\omega)$ are exactly zero below the shaded area, while they are almost zero (being several orders of magnitude lower than the shaded-area values) in the small region around $\phi = 0$, $\omega = \frac{1}{2}\pi$. The transformed lines $\theta = k\tau^2$ are shown on the same figure (the transformation of τ is in this case $\tau = \tan\phi$) and the predicted behavior of $P(\phi,\omega)$ is exhibited, with $P(\phi,\omega)$ essentially nonzero between two "transformed" lines $\theta = k_{\min}\tau^2$, $\theta = k_{\max}\tau^2$ for τ large ($|\phi| > \frac{1}{4}\pi$), while for $\tau \simeq 0$ ($\phi \simeq 0$), essentially nonzero for $\frac{1}{4}\pi \le \omega < \omega_{\max} < \frac{1}{2}\pi$. The obtained solution obeys the normalization condition (2.8) involving the probability distribution $f(\phi)$, which is itself normalized to 1. $f(\phi)$ is obtained independently of $P(\phi,\omega)$ by solving numerically the integral equation (2.5) as in Ref. 9. Finally, the probability

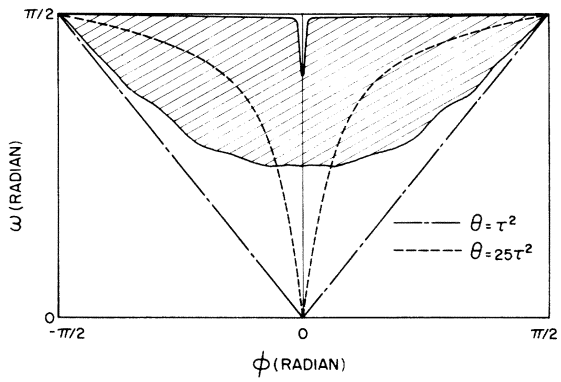

FIG. 1. Joint probability distribution $P(\phi, \omega)$ (see text) has nonzero values only in the shaded area of the ϕ-ω plane. The variables ϕ, ω are related to the original variables, τ, θ in this case, by $\tau = \tan\phi$ and $\theta = \tan^2\omega$.

distribution of θ, $P(\theta;E)$ defined in its transformed form as

$$\Pi(\omega) = \int_{-\pi/2}^{\pi/2} P(\phi, \omega)\, d\phi \tag{3.5}$$

was found to exhibit the predicted behavior at $\omega \to \frac{1}{2}\pi$ ($\theta \to \infty$) as discussed in Sec. IV of I [$P(\theta;E) \to \theta^{-3/2}$] as $\theta \to \infty$.

B. Calculation of $\langle \zeta_{0l}(E) \rangle_{av}$

In Sec. III A we have given the formulas (2.10)–(2.14) expressing $\langle \zeta_{00}(E) \rangle_{av}$ and the successive $\langle \zeta_{0l}(E) \rangle_{av}$ ($l = 1, 2, \ldots$) in terms of $P(\phi, \omega)$. It is then straightforward to calculate $\langle \zeta_{00}(E) \rangle_{av}$ from (2.10) by numerical integration using the obtained $P(\phi, \omega)$. In a similar fashion it is also possible to calculate the successive $\langle \zeta_{0l}(E) \rangle_{av}$ ($l = 1, 2, \ldots$) from (2.14). Equation (2.14), though, involves also some functions $Z_l(\phi, \omega)$ which are obtained from the relations (2.12) and (2.13). Equation (2.13) is actually an iteration scheme, capable of calculating the successive Z_l, of the form

$$Z_l = KZ_{l-1}, \tag{3.6}$$

with the kernel K qualitatively similar to the kernel K_0 in (3.4), as one can see by comparing (2.7) and (2.13); one should then expect that the iteration converges in the form

$$Z_l - uZ_{l-1} \to 0 \quad \text{as } l \to \infty, \tag{3.7}$$

where u is an eigenvalue of the kernel K. Careful study of the properties of the kernel K is required in order to obtain numerically correct limiting behavior of the iteration scheme as $l \to \infty$, basically because here, too, as with the integral equation (2.7), the behavior of each $Z_l(\phi, \omega)$ as $\omega \to \frac{1}{2}\pi$ (ω beyond the last subdivision) is required. Some analysis of (2.13) performed in a fashion similar to that used in Sec. IV of I reveals that

$$Z_l(\phi, \omega) \to (\tfrac{1}{2}\pi - \omega)^2, \quad \omega \to \tfrac{1}{2}\pi, \quad |\phi| > 0, \tag{3.8}$$

while

$$Z_l(\phi, \omega) \to (\Delta\phi)^{-1} \int_{-\Delta\phi/2}^{\Delta\phi/2} \frac{d\phi}{1 + k_0\tau^2(\phi)(\frac{1}{2}\pi - \omega)^{-2}}, \quad \omega \to \tfrac{1}{2}\pi, \ \phi \simeq 0, \tag{3.9}$$

where $\Delta\phi$ is the distance of two successive subdivisions and k_0 determines typically the line $\theta(\omega) = k_0\tau^2(\phi)$ along which $P(\phi, \omega)$ exhibits its maximum values.

With all of the above in mind we proceeded to perform the iteration and obtained the successive values of $\langle \zeta_{0l}(E) \rangle_{av}$ for the different values of energy E and degrees of disorder α. In Fig. 2 we show the obtained $\langle \zeta_{0l}(E) \rangle_{av}$ vs E for an $\alpha = 2$ (on the "high-disorder" side) for $l = 0, 1, 2, 5, 10$. We observe the gradual decay of values as l increases from zero, the decay being much faster towards the band edges. We also observe the resemblance of the shape of $\langle \zeta_{0l}(E) \rangle_{av}$, for the first few l at least, to the typical shape of an amorphous 1-D density of states. This behavior is qualitatively understood because, as discussed already, at the limit $\alpha \to \infty$ we have $\langle \zeta_{00}(E) \rangle_{av} \to \rho(E)$ (the average density of states per site). The resemblance persists for $\alpha = 0.5$ as well (on the "weak-disorder" side), although there $\langle \zeta_{00}(E) \rangle_{av}$ is an order of magnitude lower than $\rho(E)$ as shown in Fig. 3, where we present in a semilogarithmic scale values of $\langle \zeta_{00}(E) \rangle_{av}$ vs E for $\alpha = 0.5$ and $l = 0, 1, 2, 5, 6, 16, 40$, plotting also $\rho(E)$ for comparison. The important feature in this figure is the presence of strong oscillations

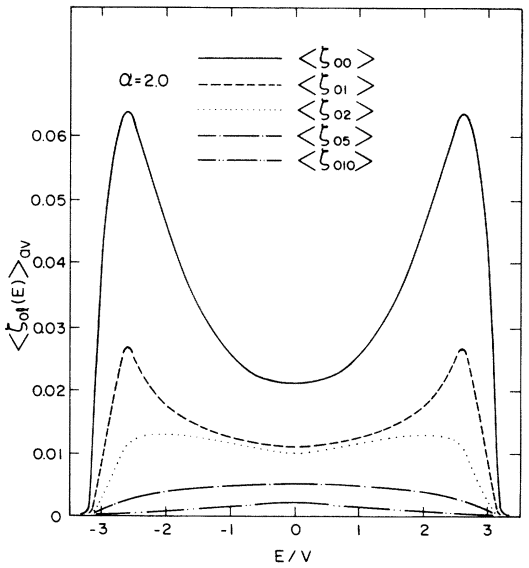

FIG. 2. Quantities $\langle \zeta_{0l}(E) \rangle_{av}$, $l = 0$, 1, 2, 5, 10, vs energy ($V = 1$) for the degree of randomness $\alpha = 2$. Note the decrease and the change of the shape as l increases.

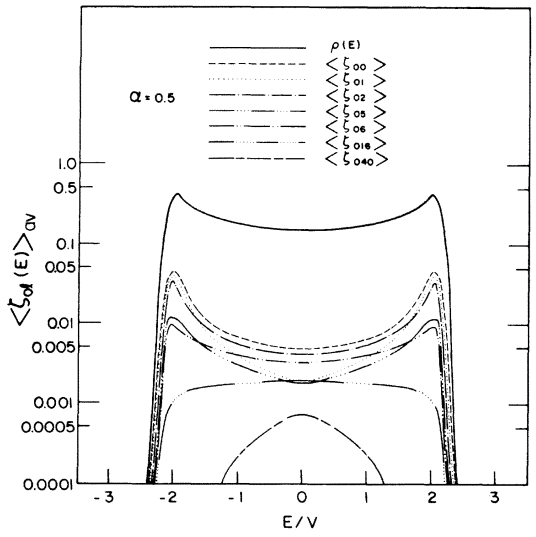

FIG. 3. Quantities $\langle \zeta_{0l}(E) \rangle_{av}$, $l=0$, 1, 2, 5, 6, 16, 40, vs energy ($V=1$) for $\alpha=0.5$. The density of states $\rho(E)$ is also presented. Note that there is little but energy-dependent change from $l=1$ to $l=6$, in contrast to the case shown in Fig. 2.

of the values of the ζ_{0l} in successive l for energies around the middle of the band, a feature absent in Fig. 2, while towards the band edges the oscillations disappear and the rate of decay of the values is much faster, causing again as in Fig. 2 a completely different shape of the curves of l small and l large.

The oscillations mentioned above are clearly understood and interpreted as caused by the phase correlation of the eigenfunction in successive sites. This phase-correlation effect is naturally strong for small degrees of disorder α; it is energy dependent and it is not wiped out by the averaging process. In order to see that correlation effect more explicitly, one should consider $\langle \zeta_{0l}(E) \rangle_{av}$ as being qualitatively an average of square amplitudes of the form $\langle a_0 \cos^2\phi_0\, a_l \cos^2\phi_l \rangle_{av}$ with, say, the ϕ_l having a flat probability distribution of values between 0 and 2π. Clearly the average value depends on the correlation of the random phases ϕ_0 and ϕ_l. If ϕ_0 and ϕ_l are strongly correlated, as in the case of small degrees of disorder and small l, then the energy-dependent phase change in successive l will appear in the average. For example, consider $l=0, 1, 2$ and an energy in the middle of a band with small disorder α. Then we have $\phi_1 \simeq \phi_0 + \frac{1}{2}\pi$, $\phi_2 \simeq \phi_1 + \frac{1}{2}\pi \simeq \phi_0 + \pi$, and $\langle \zeta_{00}(E) \rangle_{av} = \langle a_0^2 \cos^4\phi_0 \rangle_{av} \geq \langle \zeta_{02}(E) \rangle_{av} \simeq \langle a_0 a_2 \cos^2\phi_0 \times \cos^2(\phi_0 + \pi) \rangle_{av} > \langle \zeta_{01}(E) \rangle_{av} \simeq \langle a_0 a_1 \cos^2(\phi_0 + \frac{1}{2}\pi) \times \cos^2\phi_0 \rangle_{av}$. Of course such oscillations will not be seen towards the edge of the band where, even for small disorder α, the phase changes so slowly between successive sites that the disorder wipes the phase correlation out before any appreciable oscillation shows.

In general there is a phase correlation length which depends on the disorder and the energy. For l beyond that length (expressed in number of sites), the disorder wipes out any correlation between ϕ_0 and ϕ_l, the average is simply a product $\langle a_0 \cos^2\phi_0 \rangle_{av} \times \langle a_l \cos^2\phi_l \rangle_{av}$, and the energy-dependent oscillations essentially disappear. The above-described behavior is fully supported by our results and is more clearly presented in Fig. 4. There we show the values of $\langle \zeta_{0l}(E) \rangle$ vs l for two different energies and degrees of disorder.

IV. CALCULATION OF QUANTITIES OF INTEREST

A. Form of the eigenstates

In a 1-D disordered system all eigenstates are exponentially localized,[10] i.e., the modulus of their amplitude behaves at infinity ($l \to \infty$) as $\exp(-l/L_d)$, L_d (in number of sites) being the characteristic length of decay. This length clearly describes the behavior of the eigenstate in its extreme tails, i.e., far from the region where it is

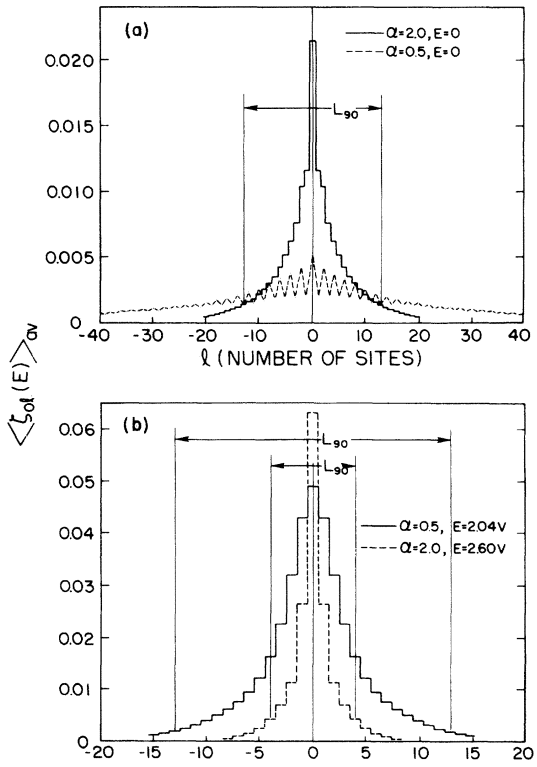

FIG. 4. Quantities $\langle \zeta_{0l}(E) \rangle_{av}$ vs l for E (a) lying at the center of the band and (b) at the band edges for two different degrees of disorder, $\alpha=0.5$ and $\alpha=2$. The length L_{90} (see text) is also shown. Note the oscillations for $\alpha=0.5$, $E=0$.

appreciable, but it is an open question whether it has any relevance to the length over which the eigenstate exhibits its appreciable values. In a system with weak disorder α, L_d behaves as α^{-2}, a behavior well established from published calculations[11] and from our present results (statements to the contrary in the literature[6] are incorrect). The α^{-2} behavior is a direct consequence of incoherent superposition of amplitudes; one can arrive at that[12-14] by a reflection-coefficient study or an equivalent mean-free-path calculation. If incoherent superposition is assumed, then[12,13]

$$L_d^{-1} \propto \langle |r|^2 \rangle_{\text{av}} \tag{4.1}$$

for $|r|^2$ small, where $|r|^2$ is the reflection coefficient from a single impurity. Then for energies at the center of the band ($E=0$)

$$|r|^2 = \epsilon^2/(4+\epsilon^2), \tag{4.2}$$

which means[15]

$$L_d^{-1}(E=0) \propto \alpha^2 \quad \text{as} \quad \alpha \to 0. \tag{4.3}$$

In the above calculation the interference terms are excluded from the beginning, the equivalent of a mean-free-path calculation where complete phase cancellation is assumed. The interference or cross terms, though, have an $|r|^1$ dependence and therefore behave as α^{-1} when $\alpha \to 0$. Therefore if they were not excluded or neglected in a calculation like the above, some α^{-1}-dependent terms would survive even in the cases of strong phase cancellation. Then α^{-1}, however small in weight, would dominate at the limit $\alpha \to 0$. The above suggests that the length L_d is insensitive to effects involving coherent superposition of amplitudes, while the eigenstate in the region where it exhibits appreciable values may be strongly influenced by interference effects, the equivalent of resonating with certain clusters of sites in the system. Therefore the typical form of an eigenstate may be far more complicated than the simple picture of a wave function almost regularly decaying at both sides, as suggested by its behavior at infinity.

The need to describe in a more realistic way the typical form of the eigenstate not in its extreme tails is important, as already pointed out. For example, often one needs to estimate the relative overlap of two eigenstates. When two eigenstates are not very far apart, their overlap may not be described at all by the overlap of their extreme tails, which is governed by L_d. To describe the eigenstate more realistically we introduced in Sec. III of I more than one characteristic length. We consider here, therefore, apart from the decay length L_d, the following lengths (all expressed in number of sites): (a) $L_{\text{eff}}(E)$ as the effective number of sites that contain the eigenstate, and (b) $L_{90}(E)$ as the number of consecutive sites over

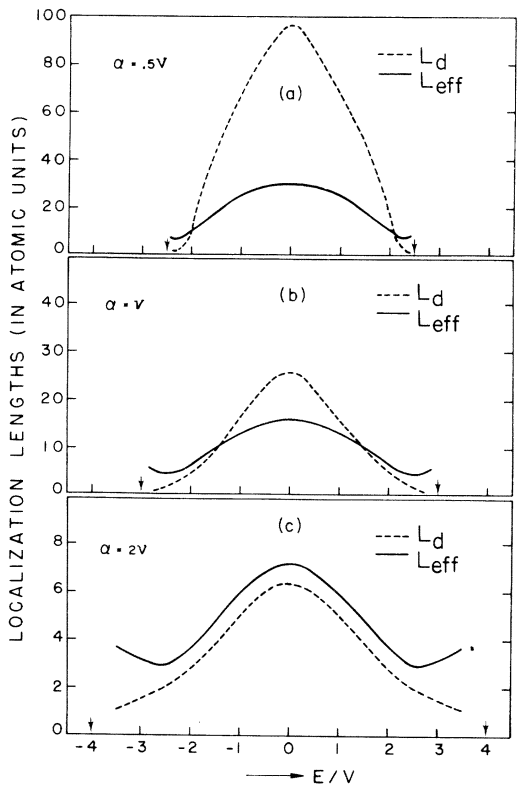

FIG. 5. Length L_{eff}, giving the total number of sites participating in the eigenfunction $|E\rangle$, and the decay length L_d vs $E(V=1)$ for three characteristic values of the degree of randomness α; (a) small randomness, $\alpha = 0.5$; (b) medium randomness, $\alpha = 1$; (c) large randomness, $\alpha = 2$.

which the 90% of the eigenstate (i.e., of the square amplitude of its eigenfunction) is contained. Both lengths can be obtained from $\langle \zeta_{0l}(E) \rangle_{\text{av}}$ and we have calculated them. In Fig. 4 we plot $\langle \zeta_{0l}(E) \rangle_{\text{av}}$ vs l for energies in the middle of the band as well as for energies close to the band edge and for two different degrees of disorder, $\alpha = 0.5$ and $\alpha = 2$. On the same figure we indicate how we define the $L_{90}(E)$ such that

$$\sum_{l=-L_{90}/2}^{L_{90}/2} \frac{\langle \zeta_{0l}(E) \rangle_{\text{av}}}{\rho(E)} = 0.9. \tag{4.4}$$

In Fig. 5 we present $L_{\text{eff}}(E)$ vs E and we plot $L_d(E)$ also for comparison. We observe that $L_{\text{eff}}(E)$ stays considerably smaller than $L_d(E)$ as α decreases. In Fig. 6 we plot and present the maximum value of $L_{\text{eff}}(L_{\text{eff}}^{\max})$, achieved for each α in the middle of the band, versus $1/\alpha$. On the same figure we also present an empirical fit of the data over the entire range from $\alpha = 0.25$ to $\alpha = 6.0$. The fitting curve is

$$L_{\text{eff}}^{\max} = 1 + (64/\alpha^2) \ln(\tfrac{1}{4}\alpha + 1), \tag{4.5}$$

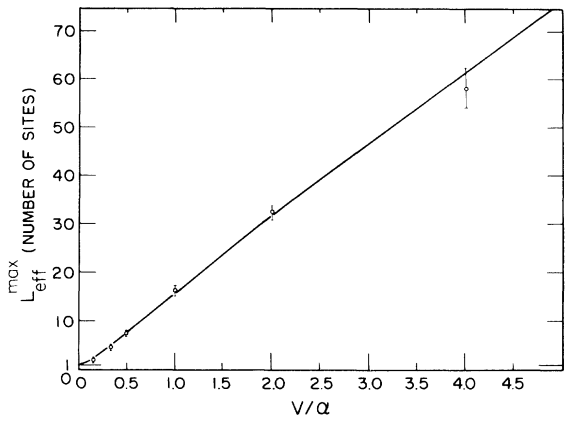

FIG. 6. Length $L_{eff}^{max} \equiv L_{eff}$ $(E=0)$ vs the inverse of the degree of randomness $\alpha(V=1)$. The points with the error bars show our numerical results. The solid line is an empirical fit (see text).

and has the limits $L_{eff}^{max} \to 1$ as $\alpha \to \infty$ and $L_{eff}^{max} \to \alpha^{-1}$ as $\alpha \to 0$. The limit $L_{eff}^{max} = 1$ is naturally correct because when the degree of disorder in the system goes to infinity the particle is localized on just one site, since with probability 1 its energy differs by an infinite amount from those of the neighboring sites. Also, as $\alpha \to 0$, $L_{eff}^{max} \to \infty$, of course, and our data suggest an α^{-k} (with $k \leq 1$) behavior for L_{eff}^{max} as $\alpha \to 0$. Numerical accuracy versus computing expense unfortunately did not allow further numerical exploration of the limit $\alpha \to 0$. Nevertheless, a quasi-α^{-1} behavior is clearly suggested for $\alpha < 2$, which indicates, as was discussed at the beginning of this subsection, that L_{eff}, unlike L_d, is strongly influenced by interference effects present in the region where the eigenstate exhibits its appreciable values. The presence of interference effects is also indicated independently from a comparison of L_{eff} and L_{90}. In Fig. 7 we plot L_{90} vs L_{eff} for different values of E and α. It is remarkable that the points seem to fit on one line instead of spreading around as is expected for quantities depending on two independent parameters E and α. We observe that L_{90} stays much larger than L_{eff} (about four times larger) for values of L_{eff} larger than 10. Recalling the definitions of L_{90} and L_{eff}, we deduce that the form of the eigenstates in the case of weak disorder (α small) has many vacancies, and the eigenstate extends over many more sites (L_{90}) than it is actually present on (L_{eff}), which again indicates the significant role of strong interference effects. In other words, the appreciable part of the eigenstate seems to be composed of clusters of sites where the eigenstate is boosted, as in the case of resonance scattering in elementary quantum mechanics,[16] separated by clusters of sites where the eigenstate has only a minimal presence.

A feature of $L_{eff}(E)$ worth special mention is exhibited in Fig. 5. That is a turn upwards of $L_{eff}(E)$ as E approaches the tails of the band. Probabilistic arguments first proposed by Lifshitz[17] suggest that eigenstates in the tails of the band should be associated with deep and extensive fluctuations in the potential. The more we approach the extreme tails, the deeper, rarer, and more extensive these fluctuations should become. As a result the density of states should decrease very fast (a feature already verified) and the extent of the eigenfunctions should increase, approaching infinity, at the exact band edges. The present results for the first time confirm directly this expected increase of the extent of the eigenfunction as we approach the extreme band edges or Lifshitz limits.

We conclude this subsection by discussing the length R_f which was introduced in Sec. III of I. This length is representing the extent of the region of the fluctuations of the eigenfunction before it starts decaying in its tails; as was remarked there, it is indirectly related to the behavior of $\langle \xi_{0l}(E) \rangle_{av}$ in the sense that $\langle \xi_{0l}(E) \rangle_{av} \to \exp[-2l/L_d(E)]$ for $l \gg R_f$ (expressed in number of sites). The observed behavior of the $\langle \xi_{0l}(E) \rangle_{av}$ is characterized by a weakly l-dependent decay length $L'(E)$ (in number of sites also), and for l around $L_{eff}(E)$, $L'(E)$

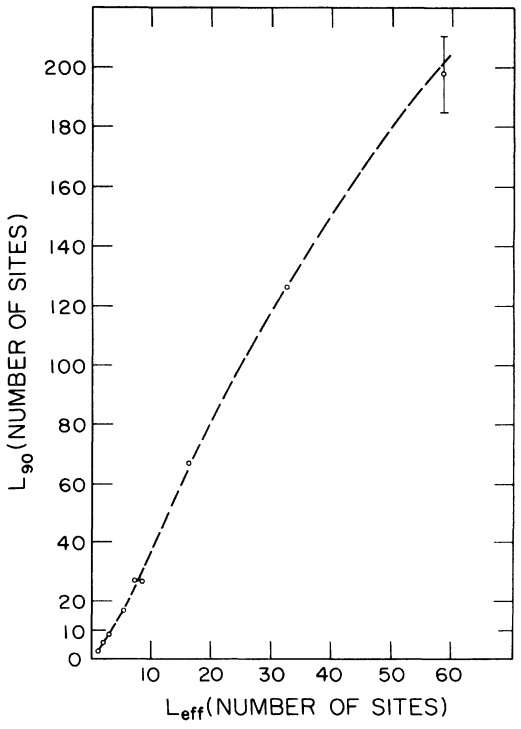

FIG. 7. Length L_{90} vs L_{eff}. The points obtained for various energies E and degrees of randomness α seem to follow a single curve which is close to a straight line.

remained always close to $L_{\text{eff}}(E)$ rather than to $\frac{1}{2}L_d(E)$. Numerical accuracy or expense did not allow a study of $L'(E)$ for $l \gg L_{\text{eff}}$ in order to observe its $\frac{1}{2}L_d(E)$ behavior and obtain, at the same time, some estimate for R_f. The only estimate we have for R_f relates to the discussion about some "phase-correlation length" given at the end of Sec. III, and in the following sense:

We solve the integral equation by an iteration procedure as already explained. This iteration procedure essentially produces successive functions P_n starting from an arbitrary P_1 [see relation (3.4)] and converges to some function P (which we accept as the solution) after a number of iterations, or steps. We argue that the number of steps necessary to obtain convergence should be closely related to that phase-correlation length (expressed, of course, in number of steps, or rather, sites) and indeed we have found this number of steps to be a characteristic number for a given E and α, with little sensitivity to the numerical details (as, e.g., the number of discrete points on the ϕ axis and the convergence accuracy). If one assumes that this number of steps describes how far we should go to eliminate any phase memory, then it is natural to relate that length with R_f, because R_f the exponential tail of the eigenfunction starts and, as already pointed out, the decay in the tail is a result of complete loss of phase memory of the eigenfunction. We have found the said number of steps to be of the same order, and a little longer than L_d for a range of L_d values in the middle of the band between 10 and 3000, while it remained larger than L_d (of the order of L_{eff}) as L_d approached zero.

In summary, four different localization lengths were studied and their implications for the form of the eigenstates discussed. The main result of our analysis is that the decay length L_d, in all cases but that of extreme localization, has little relevance to the actual extent of the appreciable part of the eigenstate, and one should be cautious when estimating overlaps of eigenstates.

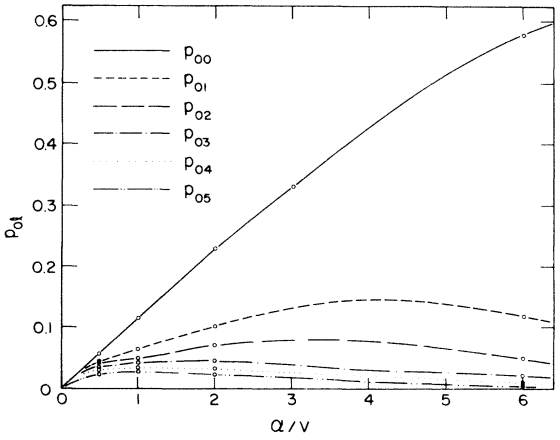

FIG. 8. Probabilities P_{0l} (see text), $l=0, \ldots, 5$, vs the degree of disorder α $(V=1)$.

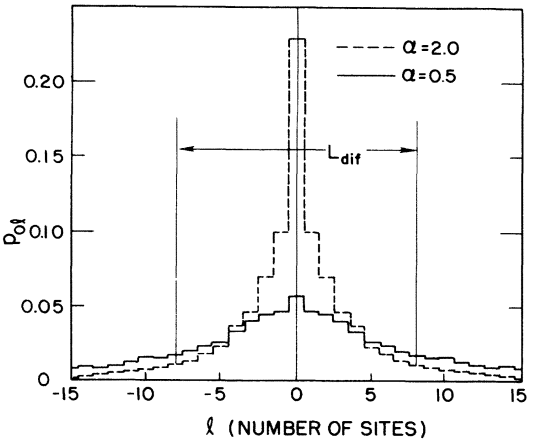

FIG. 9. Probabilities P_{0l} (see text) vs l for $\alpha=0.5$ and $\alpha=2$. The diffusion length L_{dif} is defined such that 0.9 of the area under the dashed curve ($\alpha=2$) lies between $-\frac{1}{2}L_{\text{dif}}$ and $\frac{1}{2}L_{\text{dif}}$.

B. Particle diffusibility

A quantity concerning particle diffusibility in a 1-D disordered system was also introduced in Sec. III of I. This quantity P_{0l} represents the (time-averaged) probability of discovering the particle at the state $|l\rangle$ after an infinite time has elapsed from the moment we placed the particle at the state $|0\rangle$. This quantity has therefore a clear physical meaning and can be straightforwardly calculated from the $\langle \zeta_{0l}(E) \rangle_{\text{av}}$. In Fig. 8 we present P_{0l} vs α

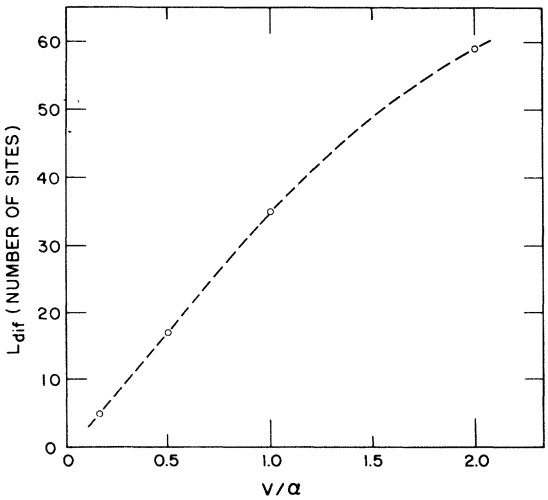

FIG. 10. Diffusion length L_{dif} vs the inverse of the degree of randomness α $(V=1)$.

for $l=0,1,2,3,4,5$. We observe the expected behavior $P_{0l}\to 0$ as $\alpha\to 0$, $l=0,1,2,\ldots$, while $P_{0l}\to 0$ as $\alpha\to\infty$, $l=1,2,\ldots$ and $p_{00}\to 1$ when $\alpha\to\infty$, as the limit of extreme localization is approached. It seems that $P_{0l}(\alpha)\propto\alpha$ as $\alpha\to 0$; in particular P_{00} seems to follow a linear dependence on α up to $\alpha\approx 3$ and bends only slightly at $\alpha=6$.

In Fig. 9 we present P_{0l} vs l for $\alpha=0.5$ and $\alpha=2.0$. We observe the change of character from "extended" to "localized" and since

$$\sum_{l=-\infty}^{\infty} P_{0l}=1\,,$$

we define a diffusibility length L_{dif} (in number of sites) as the length inside which we have a 90% (arbitrarily chosen) probability of rediscovering the particle initially placed in the middle of that length. That length, of course, goes to infinity as $\alpha\to 0$ and becomes 1 at a very high value of α. This behavior is shown in Fig. 10 where we plot L_{dif} vs $1/\alpha$ for a range of α from 0.5 to 6. A behavior α^{-k} (with $k\leq 1$) for small α is suggested by our data.

In conclusion, we have studied here for the first time various lengths characterizing the shape and extent of the eigenfunctions in 1-D disordered systems. Depending on the eigenenergy and the degree of disorder, the eigenfunctions have different shapes as well as extent. The case of low disorder and with E lying well within the band deserves particular attention because of the rather complicated form of the eigenstate. On the other hand, for high disorder or E lying in the tails of the band, the eigenfunction has a much simpler shape which agrees with intuitive pictures proposed in the past. We have also obtained results for the probabilities P_{0l}.

---

*Work supported in part by NSF Grant No. GH-37264 and a University of Virginia computing grant.

[1]C. Papatriantafillou, E. N. Economou, and T. P. Eggarter, preceding paper, Phys. Rev. B 13, 910 (1975).
[2]A. J. Epstein, S. Etemad, A. F. Garito, and A. J. Heeger, Phys. Rev. B 5, 952 (1972).
[3]I. F. Shchegolev, Phys. Status Solidi A 12, 9 (1972), and references therein.
[4]A. N. Bloch, R. B. Weisman, and C. M. Varma, Phys. Rev. Lett. 28, 753 (1972); P. F. Williams and A. N. Bloch, Phys. Rev. B 10, 1097 (1974).
[5]B. I. Halperin, in Adv. Chem. Phys. 13, 123 (1967), outlined how one can obtain an integral equation for a quantity directly related to $\langle GG^*\rangle_{\mathrm{av}}$.
[6]E. N. Economou and C. T. Papatriantafillou, Phys. Rev. Lett. 32, 1130 (1974).
[7]V. Ambegaokar, B. I. Halperin, and S. J. Langer, Phys. Rev. B 4, 2612 (1971).
[8]E. N. Economou and M. H. Cohen, Phys. Rev. B 4, 396 (1971).
[9]C. Papatriantafillou, Phys. Rev. B 7, 5386 (1973).
[10]R. E. Borland, Proc. R. Soc. A 274, 529 (1963).
[11]R. L. Bush, Phys. Rev. B 6, 1182 (1972).
[12]N. F. Mott, Adv. Phys. 16, 49 (1967).
[13]R. Landauer, Philos. Mag. 21, 863 (1970).
[14]B. Y. Tong, Phys. Rev. A 1, 52 (1970).
[15]It should be noted that by considering only the transmitted part at each site, thus neglecting the *randomly* superposed reflected part, we have

$$(|\,\text{Amplitude at } l\,|\,/\,|\,\text{amplitude at } 0\,|\,)^2=(1-|\,r\,|^2)^l$$

and

$$L_d^{-1}=\tfrac{1}{2}\langle\ln(1+|\,r\,|^2)\rangle_{\mathrm{av}}\to\tfrac{1}{2}\langle|\,r\,|^2\rangle$$

as $|\,r\,|\to 0$, which for the case of the rectangular distribution gives [using (4.2)] $L_d^{-1}\to\frac{1}{24}\alpha^2$ as $\alpha\to 0$. This is exactly the behavior exhibited by L_d in our numerical results.
[16]E. Merzbacher, *Quantum Mechanics* (Wiley, New York, 1961), pp. 102–111.
[17]I. M. Lifshitz, Usp. Fiz. Nauk 83, 617 (1964) [Sov. Phys.-Usp. 7, 549 (1965)].